

Ultrasound radiation force as a method to characterize the viscosity of microbubble shells

Outi Supponen
Mechanical Engineering
McGill University
Montreal, Canada
outi.supponen@mcgill.ca

Awaneesh Upadhyay
Mechanical Engineering
University of Colorado Boulder
Boulder, USA
awaneesh.k.upadhyay@colorado.edu

Jordan Lum
Mechanical Engineering
University of Colorado Boulder
Boulder, USA
jordan.lum@colorado.edu

Francesco Guidi
Information Engineering
University of Florence
Florence, Italy
francesco.guidi@unifi.it

Todd Murray
Mechanical Engineering
University of Colorado Boulder
Boulder, USA
todd.murray@colorado.edu

Hendrik Vos
Biomedical Engineering
Thorax Center, Erasmus MC
Rotterdam, the Netherlands
h.vos@erasmusmc.nl

Piero Tortoli
Information Engineering
University of Florence
Florence, Italy
piero.tortoli@unifi.it

Mark Borden
Mechanical Engineering
University of Colorado Boulder
Boulder, USA
mark.borden@colorado.edu

Abstract— Characterizing the complex viscoelastic properties of microbubble shells typically requires experimentally challenging techniques, such as isolating single microbubbles and measuring optically their oscillatory response to well-controlled acoustic driving. Here, we propose a relatively simple alternative method to determine the shell viscosity for a known shell elasticity, which consists of measuring ultrasound radiation force-induced displacements within freely floating microbubble populations using a standard ultrasound-imaging probe. We experimentally tested this technique on lipid-coated microbubbles and verified its accuracy by comparing with measurements made on the oscillatory response of individual microbubbles to ultrasound driving.

Keywords— *Ultrasound contrast agents, microbubbles, primary radiation force, viscoelasticity*

I. INTRODUCTION

Microbubbles have been in use as ultrasound contrast agents for decades owing to their excellent sound scattering characteristics. More recently, there have been efforts to uncover the full potential of these microbubbles in ultrasound molecular imaging and drug delivery. Their encapsulating shell, which stabilizes them against dissolution and coalescence, can be equipped with targeting ligands to bind onto sites that express disease biomarkers [1]. Localised drug deposition by ultrasound-driven microbubbles can be achieved in image-guided therapy [2]. Combined with high-intensity focused ultrasound, microbubbles can transiently disrupt the highly selective blood-brain barrier in a non-invasive way, allowing medication to reach the brain to treat neurological diseases or brain tumours [3].

To optimize the ultrasound driving conditions and the design criteria to reach the desired microbubble-induced effects, an understanding and control of the microbubble behavior under various conditions is required. Predicting the mechanics associated with oscillating ultrasound contrast agent microbubbles is not as straightforward as for bare bubbles. The

main complication arises from the mechanics of the encapsulating shell, which typically behaves in a viscoelastic manner. Different techniques have been proposed in the past to characterise the microbubble shell viscoelasticity, including optical methods such as high-speed imaging [4] and forward light scattering [5], as well as attenuation [6] and deflation [7] measurements. However, such techniques often require costly and sophisticated instrumentation able to measure at high speeds and at micro-scales, delicate alignments of such instruments, the isolation of individual microbubbles, and/or highly monodisperse microbubble size distributions.

Here, we propose an alternative technique to perform “microbubble spectroscopy” using a relatively simple setup. It consists of measuring the peak displacement produced by a microbubble population driven by a standard clinical linear-array ultrasound probe at a range of transmission frequencies. The measurements are compared with the relevant theory for microbubble displacements to find the best-fitted model parameters, in particular the shell viscosity. The proposed method is a quick and convenient way to determine the microbubble shell viscosity in-house.

II. THEORY

Microbubbles produce the largest displacements when driven into oscillations at their resonance frequency [8] with long pulses and at high driving amplitudes. The microbubble radial dynamics at high-amplitude driving are well described with a modified Herring equation with additional pressure terms to account for the bubble’s surface viscoelasticity and for the bubble translation:

$$\rho \left(R\ddot{R} + \frac{3}{2}\dot{R}^2 \right) = \left[p_0 + \frac{2\sigma(R_0)}{R_0} \right] \left(\frac{R_0}{R} \right)^{3\gamma} \left(1 - \frac{3\gamma}{c} \dot{R} \right) - \frac{4\mu\dot{R}}{R} - \frac{4\kappa_S\dot{R}}{R^2} \left(\frac{R_0}{R} \right)^2 - \frac{2\chi}{R} \left(\frac{R_0}{R} \right)^2 \left(1 - \frac{R_0}{R} \right) + \frac{\rho u^2}{4} - [p_0 + p_a(t)]. \quad (1)$$

The left-hand side of (1) includes the inertial terms of the equation, where ρ is the liquid density, R is the instantaneous bubble radius, and the over-dots indicate time derivatives. The right-hand side includes the pressure terms, which represent the contributions from the gas inside the bubble, liquid compressibility, the shell viscoelasticity, and the acoustic driving. Here, R_0 is the bubble radius at equilibrium (0.1-5 μm), p_0 is the atmospheric pressure (0.8 bar at Boulder, CO), $\sigma(R_0)$ is the initial surface tension of the bubble (0 or 0.05 N/m), γ is the polytropic exponent of the gas core (1.07), c is the speed of sound in the liquid (1500 m/s), μ is the liquid viscosity (8.9×10^{-4} Pas), κ_S is the dilatational surface viscosity (10^{-9} - 10^{-8} kg/s), χ is the surface elasticity (0.6 N/m), and \mathbf{u} is the translational velocity of the bubble. The acoustic driving pressure p_a is expressed by a sinusoidal function of time, $p_a(t) = p_{\max} \sin\left(\frac{2\pi f_0}{c} z(t) - 2\pi f_0 t\right)$ where p_{\max} is the peak negative pressure (200 kPa), f_0 is the driving frequency (3-7 MHz), and $z(t)$ is the bubble translation. Also, the effect of the translation on the radial motion of the bubble is accounted for in the second-last term on the right-hand side of (1), although this coupling effect usually becomes important only at higher driving pressures [9].

Equation (1) is combined with the translational equation of motion, where the external forces acting on the bubble include the ultrasound radiation force, viscous drag force, and the “added mass” force:

$$\frac{\partial \mathbf{u}}{\partial t} = \frac{2}{\rho V} \left(\frac{V}{c} \frac{\partial p_a}{\partial t} \mathbf{e} - \frac{1}{4} \pi C_D \text{Re} R \mu \mathbf{u} - \frac{1}{2} \rho \mathbf{u} \frac{dV}{dt} \right), \quad (2)$$

where $V = \frac{4\pi}{3} R^3$ is the instantaneous bubble volume, \mathbf{e} is the unit vector in the direction of the acoustic wave propagation, $C_D = \frac{24}{\text{Re}} + \frac{6}{1+\sqrt{\text{Re}}} + 0.4$ is the drag coefficient of a sphere, and $\text{Re} = \frac{2R\rho|\mathbf{u}|}{\mu}$ is the translational Reynolds number. The history term is omitted from (2) as both the radial and translational Reynolds number at resonant conditions for the driving parameters considered here are generally above 5, which is a regime where history effects have been shown to have little effect on the peak displacements [10]. Only resonant bubbles are considered in this work.

Equations (1) and (2) are solved with a variable-step, fourth-order Runge-Kutta method to finally provide the bubble’s translational velocity \mathbf{u} and the resulting translation within a single pulse.

III. METHODS

A. Microbubble synthesis

The microbubbles were produced in the laboratory and had a perfluorobutane gas core, encapsulated within a phospholipid monolayer coating (DSPC:DSPE-PEG2000 = 9:1). The microbubbles were produced by sonicating the surface of the lipid solution with a sonicator probe while simultaneously flowing perfluorobutane gas over the surface. The microbubbles were “washed” from residual lipids and from the larger bubbles through differential centrifugation [11],

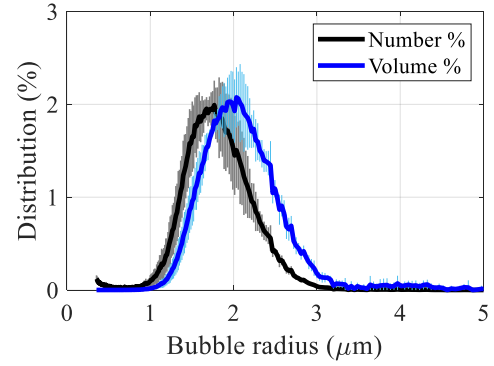


Fig. 1. Number and volume distributions of the tested microbubble population.

producing a final size distribution peaking at 1.5 to 2- μm radius, as visible in Fig. 1.

B. Experimental setup

A schematic of the experimental setup is shown in Fig. 2. A microbubble population was diluted with 0.8 L of purified water to a concentration of $5 \times 10^4 \text{ mL}^{-1}$. The suspension was insonified with a linear-array ultrasound probe (LA332) driven by an ultrasound open platform (ULA-OP) with 10- μs pulses at 4-kHz pulse repetition frequency (PRF) and at 200-kPa peak negative pressure. The transmission driving frequency was varied between 3 and 7 MHz. Plane wave transmission was used to apply a uniform pressure along a large range of depths [12], increasing the probability to capture a resonant bubble at the applied peak negative pressure. The microbubble displacements along the axis of the insonified region were acquired from the frequency shifts in the measured echo signals using the multi-gate spectral Doppler approach. For each condition, the maximum frequency shift Δf_{\max} within an acquisition of 240,000 echoes was recorded, corresponding to the peak microbubble displacement (PMD) within a pulse through the relation $\text{PMD} = \frac{\Delta f_{\max} c}{2 f_0 \text{PRF}}$. Further details on the Doppler measurements may be found in [13].

The measured PMDs were compared with theoretical peak displacements computed by the coupled equations (1) and (2).

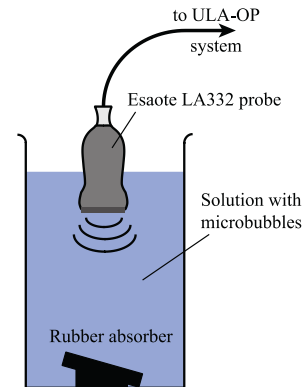


Fig. 2. Schematic of the experimental setup.

With the assumption of a constant surface elasticity, the best-fitted surface viscosity κ_s was determined by assuming the measured PMD to correspond to the theoretical resonant bubble size at each driving frequency.

C. Shell characterization on individual microbubbles

In a separate setup [5], the surface elasticity and viscosity were determined on individual microbubbles to validate the method proposed in this study. Forward laser scattering was used to measure the oscillatory response of an isolated microbubble to ultrasound driving across a range of frequencies. The ultrasound driving was generated through the photoacoustic effect using an amplitude-modulated continuous wave laser heating up a liquid volume near the microbubble and resulting thus in acoustic waves at ultrasonic frequencies. The surface elasticity was obtained through the observed resonance frequency yielding highest oscillation amplitudes, and surface viscosity was characterized through the damping behavior. Further details on this reference measurement technique can be found in [5].

IV. RESULTS

Quantified using the reference photoacoustic technique, the best-fitted surface elasticity was found to remain approximately constant at 0.6 ± 0.1 N/m for a range of radii. Two values for the initial surface tension were tested: $\sigma(R_0) = 0$ N/m, which complies with the long-term stability of the bubble, and $\sigma(R_0) = 0.05$ N/m, which has been used for phospholipid shells in the past [8,10]. The viscosity was in the range of 6×10^{-9} - 4×10^{-8} kgs/s, dependent on the bubble radius within the range 1.5-4 μm , see Fig. 5.

A. Theoretical microbubble displacements

Theoretical microbubble displacements computed using (1) and (2) are shown in Fig. 3 as a function of the equilibrium bubble radius R_0 for a range of surface viscosities κ_s . For each surface viscosity, there is a peak microbubble displacement associated with a resonant bubble size. At low surface viscosities, nonlinear harmonic behavior is observed as a smaller local peak in displacement for a larger bubble radius.

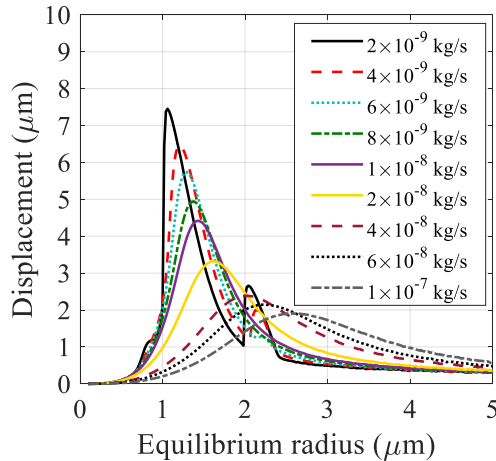


Fig. 3. Theoretical microbubble displacements, as numerically computed through (1) and (2), as a function of radius for a range of surface viscosities. Here, $f_0 = 4$ MHz and $\sigma(R_0) = 0$ N/m.

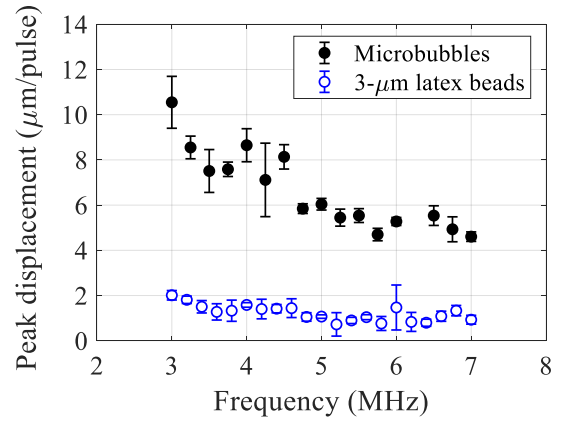


Fig. 4. Measured peak displacements of microbubbles and latex beads as a function of frequency. The latex beads quantify the contribution of acoustic streaming to the microbubble displacements. The error bars show the standard deviation from three measurements.

Overall, increasing surface viscosity yields smaller peak displacements and a larger resonant bubble radius.

B. Measured microbubble displacements

Figure 4 shows the measured peak microbubble displacements as a function of frequency. The peak displacements decrease with increasing frequency, which is explained by the smaller bubbles resonating at high frequencies displacing less compared to the larger bubbles resonating at low frequencies [8]. The contribution of acoustic streaming to the measured microbubble velocities can be important in plane wave transmission where a large volume of fluid is insonified. Therefore, the Doppler measurements were also performed measuring the displacement of tracking particles (3- μm -diameter latex beads) in the absence of bubbles. Non-negligible displacements, up to 2 μm per pulse, were measured due to streaming. These streaming velocities were subtracted from the microbubble displacements displayed in Fig. 4 to obtain the contribution from the ultrasound radiation force.

C. Characterizing microbubble surface viscosity

To characterize the surface viscosity of microbubbles, the peak displacement measurements from Fig. 4 (after subtracting streaming velocities) were compared with the theoretical microbubble displacements as displayed in Fig. 3. For example, at 4-MHz driving frequency, a peak microbubble displacement of approximately 7 $\mu\text{m}/\text{pulse}$ is measured, which corresponds to a surface viscosity between 2×10^{-9} and 4×10^{-9} kg/s and to a resonant bubble size of 1.2 μm according to Fig. 3. Such combinations of surface viscosities and resonant bubble radii for all the tested driving frequencies are plotted in Fig. 5. The error bars represent the ranges covered by the surface viscosity and bubble radius when accounting for the standard deviation of the peak microbubble displacement measurements in Fig. 4.

The surface viscosity varied with equilibrium bubble radius following approximately a logarithmic increase. This behavior is explained by the rheological shear-thinning of the lipid shell at faster dilatation rates, which increases for decreasing bubble

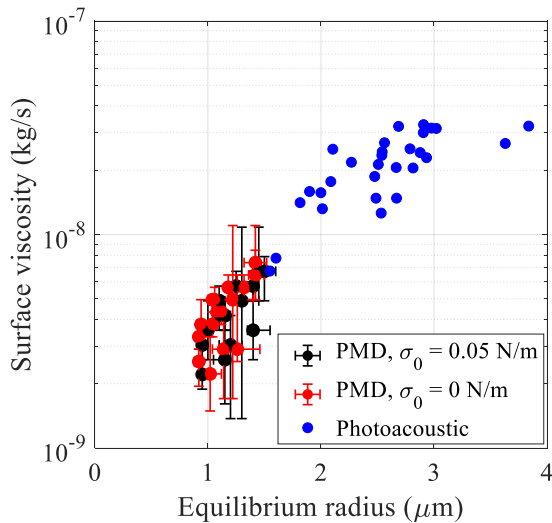


Fig. 5. Surface viscosity versus equilibrium bubble radius, extracted from best fits of (2) with and without a finite initial surface tension to peak microbubble displacement (PMD) measurements. The error bars show the ranges of R_0 and κ_S covered by the standard deviations in the PMD measurements in Fig. 4. Surface viscosity obtained through photoacoustic measurements on individual bubbles are displayed for comparison.

size. The exact mechanism causing such behavior is currently unknown. The shell viscosity varied between 2×10^{-9} and 8×10^{-9} kg/s within the radius range 0.9 to 1.5 μm , and little difference was found between the fitting procedures with and without the inclusion of an initial surface tension. Although there is little overlapping between the ranges of radii covered by these two distinct measurement techniques, the common trend agrees well with previously reported observations [4].

V. DISCUSSION AND CONCLUSION

The method outlined in this work to characterize the surface viscosity of ultrasound contrast agent microbubbles (with known surface elasticity) has many advantages. It is relatively simple in the sense that only a calibrated standard medical ultrasound probe is needed to insonify a freely floating microbubble population contained in a beaker. No sophisticated alignments are needed for the setup apart from the exclusion of acoustic reflections from the container boundaries. This technique requires no observations on individual bubbles, which are typically troublesome to isolate and to observe through ultra-high-speed measurements. Furthermore, there is no need for a highly monodisperse microbubble population; a polydisperse microbubble population is, on the contrary, favorable in order to always include the resonant bubble size. In addition, within the tested driving frequency range of 3-7 MHz, the resonant bubble size ranges within 0.9-1.5 μm radius, which is so small that it

would otherwise require extremely sophisticated measurement techniques to characterize using isolated individual bubbles. These results demonstrate an alternative technique to provide easier and more accessible microbubble characterization in a typical ultrasonics laboratory.

ACKNOWLEDGMENTS

Funding for this work was provided by NIH R01 CA195051. O.S. acknowledges the support of the Swiss National Science Foundation under grant n. P2ELP2-178206. We thank Professor John Allen for insightful discussions.

REFERENCES

- [1] Zhao S., Borden M., Bloch S.H., Kruse D., Ferrara K.W., Dayton P.A., "Radiation-force assisted targeting facilitates ultrasonic molecular imaging", *Mol Imaging*, 3(3), pp.135-148, 2004.
- [2] Lum A.F., Borden M.A., Dayton P.A., Kruse D.E., Simon S.I., Ferrara K.W. "Ultrasound radiation force enables targeted deposition of model drug carriers loaded on microbubbles", *J Control Release*, 111(1-2), pp.128-134, 2006.
- [3] Song K.-H., Harvey B.K., Borden M.A., "State-of-the-art of microbubble-assisted blood-brain barrier disruption", *Theranostics*, 8(16), pp.4393-4408, 2018.
- [4] van der Meer S., Dollet B., Voormolen M., Chin C., Bouakaz, A., de Jong N., Versluis M., and Lohse D., "Microbubble spectroscopy of ultrasound contrast agents", *The Journal of the Acoustical Society of America* 121(1), pp. 648–656, 2007.
- [5] Lum J., Stobbe D., Borden M., and Murray T., "Photoacoustic technique to measure temperature effects on microbubble viscoelastic properties", *Applied Physics Letters* 112(11), 111905, 2018.
- [6] Segers T., Gaud E., Versluis M., and Frinking P., "High-precision acoustic measurements of the nonlinear dilatational elasticity of phospholipid coated monodisperse microbubbles", *Soft Matter*, vol. 14, no. 47, pp. 9550–9561, Dec. 2018.
- [7] Guidi F., Vos H., Mori R., de Jong N., Tortoli P., "Microbubble characterization through acoustically-induced deflation", *IEEE Trans. Ultrason., Ferroelect., Freq. Contr.*, 57(1), pp.193-202, 2010.
- [8] Vos H., Guidi F., Boni E., and Tortoli P., "Method for microbubble characterization using primary radiation force", *IEEE Transactions on Ultrasonics, Ferroelectrics, and Frequency Control*, 54(7), p.1333, 2007.
- [9] Doinikov, A.A., "Translational motion of a spherical bubble in an acoustic standing wave of high intensity", *Physics of Fluids*, 14(4), p.1420, 2002.
- [10] Acconcia C., Wright A., and Goertz D., "Translational dynamics of individual microbubbles with millisecond scale ultrasound pulses", *The Journal of the Acoustical Society of America* 144(5), p.2859, 2018.
- [11] Feshitan J. A., Chen C. C., Kwan J. J., and Borden M. A., "Microbubble sie isolation by differential centrifugation," *J. Colloid Interface Sci.*, 329(2), pp. 316-324, 2009.
- [12] Blue L., Guidi F., Vos H., Slagle C., Borden M., and Tortoli P., "Plane-wave contrast imaging: A radiation force point of view", *IEEE Transactions on Ultrasonics, Ferroelectrics, and Frequency Control* 65(12), pp. 2296–2300, 2018.
- [13] Guidi F., Supponen O., Upadhyay A., Vos H., Borden M., and Tortoli P., "Microbubble radiation force-induced translation in plane-wave versus focused transmission modes", *IEEE Transactions on Ultrasonics, Ferroelectrics, and Frequency Control*, in press, 2019.